nanomaterials

MDPI

Communication

Methane-Mediated Vapor Transport Growth of Monolayer WSe_2 Crystals

Hyeon-Sik Jang [1,†], Jae-Young Lim [1,†], Seog-Gyun Kang [1], Sang-Hwa Hyun [2], Sana Sandhu [1], Seok-Kyun Son [3], Jae-Hyun Lee [2,*] and Dongmok Whang [1,*]

1 School of Advanced Materials Science and Engineering and SKKU Advanced Institute of Nanotechnology (SAINT), Sungkyunkwan University (SKKU), 2066, Seobu-Ro, Jangan-Gu, Suwon-Si, Gyeonggi-Do 16419, Korea; dagu1821@skku.edu (H.-S.J.); limjyyy@skku.edu (J.-Y.L.); suggyoon@skku.edu (S.-G.K.); sanasandhu_7@yahoo.co.in (S.S.)

2 Department of Energy Systems Research and Department of Materials Science and Engineering, Ajou University, Suwon, Gyeonggi-Do 16499, Korea; ruche@ajou.ac.kr

3 Department of Physics, Mokpo National University, Muan-gun, Jeollanam-Do 58554, Korea; skson@mokpo.ac.kr

* Correspondence: jaehyunlee@ajou.ac.kr (J.-H.L.); dwhang@skku.edu (D.W.); Tel.: +82-31-210-2465 (J.-H.L.); +82-31-290-7399 (D.W.)

† These authors contributed equally to this work.

Received: 28 October 2019; Accepted: 13 November 2019; Published: 19 November 2019

Abstract: The electrical and optical properties of semiconducting transition metal dichalcogenides (TMDs) can be tuned by controlling their composition and the number of layers they have. Among various TMDs, the monolayer WSe_2 has a direct bandgap of 1.65 eV and exhibits p-type or bipolar behavior, depending on the type of contact metal. Despite these promising properties, a lack of efficient large-area production methods for high-quality, uniform WSe_2 hinders its practical device applications. Various methods have been investigated for the synthesis of large-area monolayer WSe_2, but the difficulty of precisely controlling solid-state TMD precursors (WO_3, MoO_3, Se, and S powders) is a major obstacle to the synthesis of uniform TMD layers. In this work, we outline our success in growing large-area, high-quality, monolayered WSe_2 by utilizing methane (CH_4) gas with precisely controlled pressure as a promoter. When compared to the catalytic growth of monolayered WSe_2 without a gas-phase promoter, the catalytic growth of the monolayered WSe_2 with a CH_4 promoter reduced the nucleation density to 1/1000 and increased the grain size of monolayer WSe_2 up to 100 μm. The significant improvement in the optical properties of the resulting WSe_2 indicates that CH_4 is a suitable candidate as a promoter for the synthesis of TMD materials, because it allows accurate gas control.

Keywords: TMD; 2D material; WSe_2; monolayer; methane promoter; single-crystal

1. Introduction

The discovery of graphene and its unique properties has triggered the development of various types of layered materials [1]. In particular, transition metal dichalcogenides (TMDs), atomically thin semiconductors of the type MX_2 (M = Mo, W; X = S, Se), have attracted considerable attention as their physical and electrical properties are tunable. Depending on their composition and thickness, two-dimensional (2D) TMDs have a variety of electrical properties ranging from metal, to insulator, to semiconductor, which could lead to a new dimension of atomic thickness for future device applications [2,3]. TMD materials have useful device characteristics, such as a high on/off ratio, a wide range of photoluminescence, and a low subthreshold voltage, making them suitable for spintronics and

optoelectronics [4]. Among the numerous TMD materials, WSe_2 has been extensively studied because its electrical transport properties can be easily adjusted from p-type to bipolar behavior depending on the type of contact metal [5–7]. Bulk WSe_2 crystallizes in the "2H" or trigonal prismatic structure (space group $P6_3/mmc$; a = 0.330 nm, c = 1.298 nm), in which each W atom is surrounded by six Se atoms, defining two triangular prisms. It was also reported that the energy band structure of WSe_2 can be altered according to its layer number. WSe_2 shows a direct bandgap of 1.65 eV in the monolayer, compared to an indirect bandgap of 1.2 eV in the multilayered bulk [8,9]. Similar to another 2D layered material, TMD is typically prepared using a mechanical exfoliation method. However, this top-down approach is not suitable for practical high-performance device applications, so bottom-up approaches for large-scale and mass-production have been extensively studied. The chemical vapor deposition (CVD) method is one of the bottom-up approaches that allows the synthesis of large-area TMDs. The CVD growth of TMDs has largely been studied using two different approaches. The first approach is to pre-deposit transition metal sources such as MoO_3, WO_3, etc., on the growth substrate and convert them to TMD by sulfidation (or selenization) [10–18]. The second is a noncatalytic growth method, in which a transition metal source and sulfur (or selenium) are heat-treated in a growth tube and flowed in a gaseous state to synthesize the TMD layer on a target substrate [19,20]. However, these CVD approaches have not been successful in uniform, high-quality TMD synthesis because it is difficult to control the thickness and nucleation density of TMDs [21]. Recently, to overcome such problems, many researchers have studied various types of promoters and methods applied for CVD-based TMD synthesis to control gas-phase transport of precursors and the reaction of TMD on the growth substrate [22–26]. Ling et al. reported the synthesis of highly- crystalline MoS_2 at a relatively low growth temperature (650 °C) using various aromatic molecules as seeding promoters [13]. In particular, domain size of MoS_2 increased up to 60 μm through vaporized aromatic-molecule catalysts such as perylene-3,4,9,10- tetracarboxylic acid tetrapotassium salt (PTAS) and $F_{16}CuPc$. They also reported that uniform monolayer MoS_2 can be synthesized on the entire area of the SiO_2/Si substrate; however, the use of such an organic catalyst leaves a residue on the growth substrate that acts as a defect of the synthesized TMD. Another limitation of this method is that it is not applicable to the growth of WS_2 and WSe_2, which require high growth temperatures. In addition, inorganic materials were also reported in assisted WSe_2 growth methods [15,27]. Liu et al. demonstrated a Cu-assisted self-limited growth (CASLG) method that allowed the synthesis of a high-quality, uniform WSe_2 monolayer while maintaining a balance between high crystallinity and fast growth rates. They explained that Cu atoms, which occupy the hexagonal sites positioned at the center of the six-membered rings of the WSe_2 surface, induce self-limited growth of WSe_2 and prevent unwanted reactions [15]. However, this approach also had disadvantages, for example, the synthesized WSe_2 had small grain sizes with multilayered regions and the vapor pressure of the solid catalyst could not be precisely controlled.

Herein, we report a catalytic growth of the large-area monolayer WSe_2 by utilizing CH_4 (methane) with precisely controlled pressure as t promoter. Through a systematic investigation, it is confirmed that grain size and the nucleation density of WSe_2 can be controlled according to the ratio of carrier gases (Ar/CH_4). The gas promoter leads to synthesis of about 100 μm size domains of WSe_2 and significantly reduces nucleation density from 1.6×10^5 to 1.5×10^2 mm^{-2}. Various analytical tools such as Raman, photoluminescence (PL), X-ray photoelectron spectroscopy (XPS), and atomic force microscopy (AFM) analysis are used to demonstrate the properties of synthesized monolayer WSe_2.

2. Materials and Methods

2.1. Preparation

The WSe_2 precursor powders (Alfa Aesar, Ward Hill, MA, U.S., 99.8%; metal basis, 10 microns) were placed on the cleaned alumina boat. Prior to the growth, the SiO_2/Si wafer (thermal oxide wafer: 300 nm SiO_2 layer on Si (100), MTI Inc., Richmond, CA, U.S.) substrate was washed by acetone, ethyl alcohol, and deionized (DI) water, for 5 min, to remove the organic residue and was then treated with

oxygen plasma (100 sccm, 100 W). High-purity Ar gas (99.999%, JC gas Inc.) and methane gas diluted in Ar (1% CH_4, 99% Ar, JC gas Inc., Suwon-si, Gyeonggi-do, Korea) were used as carrier gases.

2.2. Synthesis of WSe_2

The homemade CVD system was designed to flow gas in both directions with a three-zone furnace and a double-quartz tube (outer: 34 mm diameter, inner: 15 mm diameter tube). The WSe_2 powders were placed in an alumina boat located at the center furnace of the homemade CVD. The SiO_2/Si substrate was cut to 1 cm × 5 cm size and then placed in the left furnace, about 10 cm from the alumina boat. The CVD system was pumped to the base pressure (2×10^{-3} torr) by a rotary pump for 10 min and then filled with Ar gas to 760 torr. In the process of increasing the temperature to the WSe_2 growth temperature, the flow direction of the carrier gas (Ar 200 sccm) was reversed to prevent unwanted deposition. After the temperature reached 1050 °C, the flow direction of the carrier gas was reversed again to allow the evaporated precursor to reach the growth substrate. In the synthesis process, the experiment was carried out by flowing a different ratio of Ar and CH_4 (1% diluted at Ar) for 60 min at atmospheric pressure. After the reaction, the furnace was quenched down to room temperature while maintaining the gas flow, and the samples were collected for characterization.

2.3. Characterzaion of Synthesized WSe_2

The morphology and size of synthesized WSe_2 samples were characterized using optical microscopy (OM, Olympus DX51, Tokyo, Japan) and a SEM (JEOL JSM-7401F, JEOL, LTD, Tokyo, Japan) operating at 5 kV and 10 μA. The nucleation density and grain size of WSe_2 were analyzed using the Image J program tool. The thickness and surface potential of the WSe_2 monolayer were confirmed by atomic force microscopy and Kelvin probe force microscopy (KPFM) using Park NX10 (Park system, Suwon-si, Gyeonggi-do, Korea) with a Si cantilever Pt-coated tip. X-ray photoelectron spectroscopy analysis was carried out by ESCA2000 spectrometry (Termo Fisher Scientific, Walthan, Massachusetts, U.S.) using monochromatic Al-Kα radiation (1468.6 eV). Raman and photoluminescence spectra were collected with micro-Raman spectroscopy (WITEC Raman system, Ulm, Germany) using a 532 nm laser.

3. Results and Discussion

As shown in Figure 1a, monolayer WSe_2 was synthesized on the SiO_2/Si substrate by a homemade three-zone furnace CVD using WSe_2 powder as a precursor. Briefly, the CVD system can control the temperature at each zone and adjust the direction of the carrier gas as required. During the ramping process for increasing the temperature of the furnace, the carrier gas flowed from the right to left direction to prevent the evaporated precursor from reaching the growth substrate, and the flow direction of the carrier gas was reversed during the growth process to synthesize the WSe_2 monolayer. A 1 × 5 cm^2 SiO_2/Si growth substrate was placed 10 cm away from the alumina boat containing the precursor. The growth behavior of WSe_2 was investigated by observing the product at the same location as the growth substrate, because the morphology and density of the WSe_2 crystals depended upon the distance between the precursor and the growth substrate [12,16]. Figure 1b illustrates the catalytic growth of WSe_2 crystals via vapor-solid transport mechanism, when CH_4 gas diluted in Ar (1% CH_4, 99% Ar) was used as both a carrier gas and a promoter. Like other catalysts for the growth of 2D materials, such as the Cu substrate commonly used for graphene growth, CH_4 induces the lateral epitaxy growth of WSe_2, increasing its grain size while suppressing its vertical growth or deposition. During the synthesis of WSe_2, methyl radicals and hydrogen are produced by thermal decomposition of CH_4 at the precursor hot zone (1050 °C) [28]. Methyl radicals can react with oxygen atoms on the SiO_2 surface to form O-CH_3, reducing the nucleation site of WSe_2. In addition, carbon-related radicals can react with the unstable W vapor to form metastable metallo-organic compounds, which may induce growth of low-defect WSe_2 crystals. Hydrogen is also known to induce the growth of low-defect WSe_2 crystals while suppressing vertical growth into bilayers and multilayers by etching defective WSe_2 [29–31]. Figure 1c,d show that while randomly distributed triangular WSe_2 crystals were grown,

the size, density, and thickness uniformity of the grown crystal domains varied significantly with or without CH_4 promoters. When WSe_2 was grown without CH_4 gas, grain size of the obtained domains was less than 1 μm and there were many multilayer regions (Figure 1c). However, when CH_4 gas was used as a promoter, WSe_2 existed mostly as a monolayer with a grain size of more than 10 μm (Figure 1d). These results clearly show that CH_4 gas acts as a promoter for the growth of WSe_2 crystals.

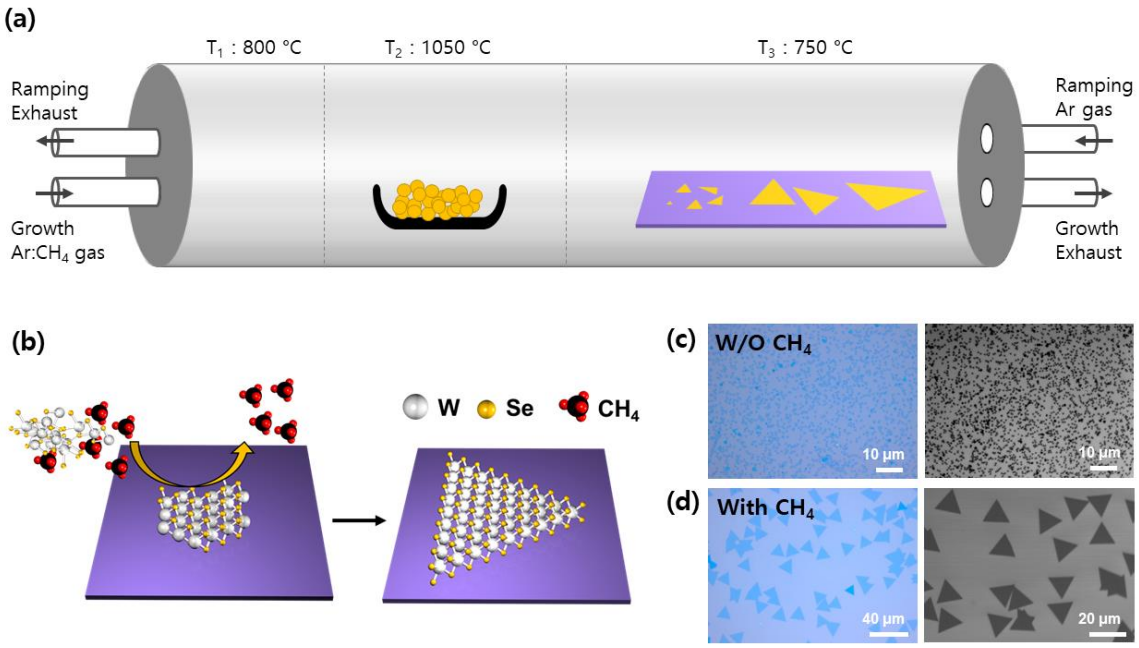

Figure 1. The schematic illustration of methane-mediated WSe_2 synthesis. (**a**) Sketch of homemade tube-type chemical vapor deposition (CVD) setup. (**b**) Schematic image of WSe_2 crystal growth by vapor-solid transport mechanism and its growth morphology difference between (**c**) without and (**d**) with methane (CH_4) gas.

As various parameters affect the CVD growth of TMDs, substrate size, carrier gas velocity, weights of precursor powders, growth time, and characterization regions were set as constant [8,10,13,18,19,22,26]. Based on this, Figure 2a–d show SEM images of WSe_2 according to the CH_4 gas ratio. Figure 2a and Figure S1 show that the WSe_2 grain size is less than 1 μm when only Ar gas is used as the carrier gas. Figure 2a and Figure S1 also show some parts of the multilayer WSe_2 regions (dark-colored) with a nucleation density of 1.6×10^5 mm^{-2}. By increasing the CH_4 gas to 50 sccm, the average grain size of WSe_2 was increased to ~6 μm with a triangular shape and a nucleation density of 5.5×10^3 mm^{-2} (Figure 2b and Figure S2). As the flow of CH_4 gas was increased to 100 sccm, the synthesized monolayer WSe_2 showed an average grain size of 9 μm with a nucleation density of 6.8×10^2 mm^{-2} (Figure 2c and Figure S3). Figure 2d and Figure S3 show that the domain size of a single crystal monolayer of WSe_2 increased up to 80 μm when flowing 150 sccm of diluted CH_4 gas. In this case, the average grain size was 52 μm with a wide distribution due to a lower nucleation density of 156 mm^{-2}. From a statistical analysis of domain images in Figures S1–S4, grain size and nucleation density of WSe_2 were obtained as a function of the CH_4 gas ratio (Figure 2e and Figure S5). Generally, increasing the CH_4 gas ratio yielded a lower nucleation density of monolayer WSe_2 with a larger grain size. The catalytic effect of CH_4 on the synthesis of large-grain monolayer WSe_2 was similar to the catalytic growth of other 2D materials (graphene, h-BN, MoS_2, WSe_2, etc.) [11,15,32–36].

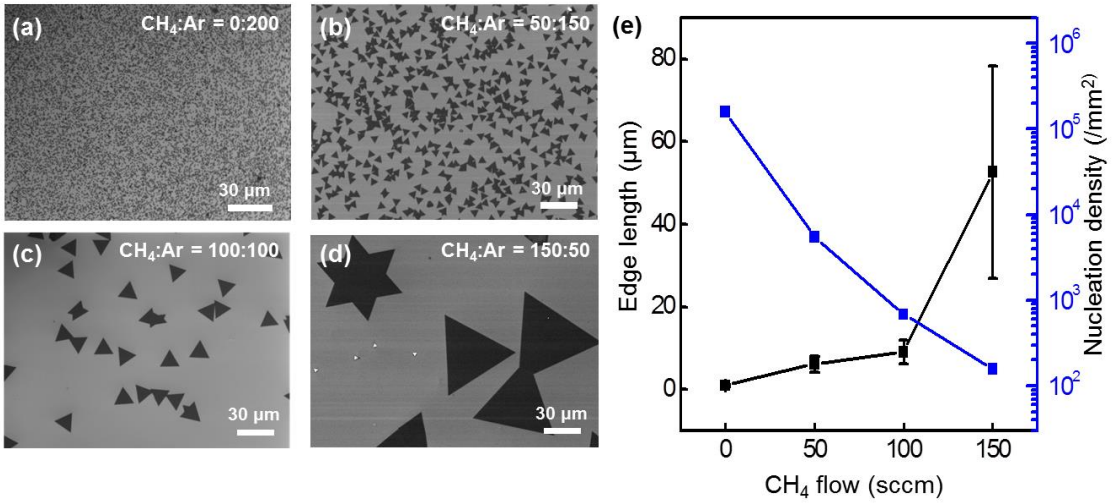

Figure 2. Size control of the WSe_2 domain by tuning the methane carrier gas ratio. Typical SEM images of WSe_2 grains synthesized on a SiO_2/Si substrate with a flow of (**a**) CH_4:Ar = 0:200, (**b**) CH_4:Ar = 50:150, (**c**) CH_4:Ar = 100:100, and (**d**) CH_4:Ar = 150:50 sccm. (**e**) Edge length (black) and nucleation density (blue) of WSe_2 domains as a function of the CH_4 gas ratio. The error bars represent the edge length variations of WSe_2 domains obtained at the same CH_4 gas flow.

We also investigated the effects of the CH_4 promoter on the morphological and optical properties of synthesized WSe_2 via the nondestructive analysis tools of Raman spectroscopy and PL. Figure 3a,b show the typical Raman mapping (at center wavelength: ~252 cm^{-1}) obtained with and without the CH_4 promoter, respectively. When CH_4 was used as a carrier gas, the grain size was about 80 μm with a uniform and strong intensity of E^1_{2g} peak over the synthesized WSe_2 crystals (Figure 3a). This result is consistent with the SEM results in Figure 2d. On the other hand, when only Ar was used as the carrier gas, the intensities of the measured E^1_{2g} peaks were much lower and nonuniform (Figure 3b). Figure 3c shows the differences in the typical Raman spectra of WSe_2 crystals grown with and without a CH_4 promoter. In the case of CH_4-assisted growth, Raman peaks corresponding to E^1_{2g} and A_{1g} modes of single-layered WSe_2 were observed (Figure S6). When only Ar gas was used, a relatively low E^1_{2g} peak and an additional small peak at 307 cm^{-1} (corresponding to B^1_{2g} resonance mode of WSe_2) were observed. In general, the B^1_{2g} peak is only active on the bilayer or multilayer of WSe_2 [5,37]. We also noted that carbon-related Raman signals such as D peak (~1350 cm^{-1}), G peak (~1600 cm^{-1}), or 2D peak (~2700 cm^{-1}) were not observed. These results indicate that CH_4 acted only as a promoter during WSe_2 synthesis and did not leave other carbon-related residues. We noted that the WSe_2 growth temperature (700~750 °C) was too low to form a carbon layer by the reaction of methane on the surface of the SiO_2/Si substrate [38]. The optical properties of the synthesized WSe_2 and the effect of the CH_4 promoter were further investigated using micro-PL with a 532 nm laser.

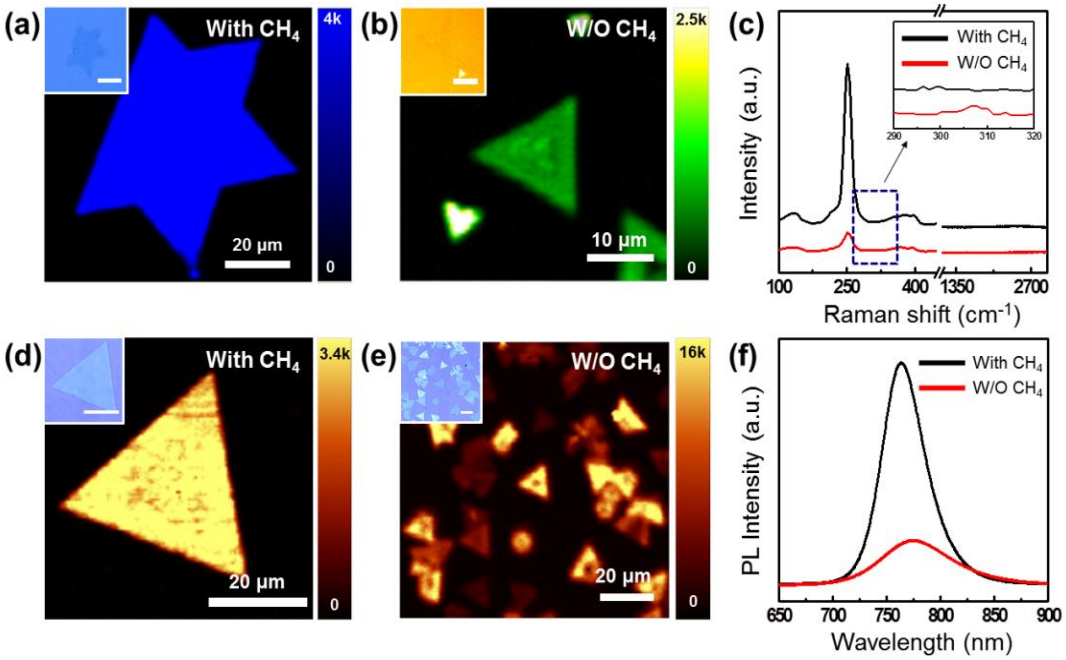

Figure 3. Raman and photoluminescence (PL) investigation of the synthesized WSe_2 according to the catalytic effects of methane. Raman mapping results of (**a**) CH_4:Ar = 150:50 sccm, (**b**) Ar gas only as carrier gas, and (**c**) representative Raman spectrum of each mapping result. PL mapping results of (**d**) CH_4:Ar = 150:50 sccm, (**e**) Ar gas only as carrier gas, And (**f**) representative PL spectrum of each mapping result. Raman and PL results were obtained from a micro-Raman instrument with a wavelength of 532 nm laser. Inset is an OM image corresponding to each mapping region.

Figure 3d shows the PL mapping of WSe_2 synthesized using a CH_4 promoter (CH_4:Ar = 150:50). The synthesized WSe_2 grain exhibited a uniform PL intensity at the 760 nm wavelength, which is equivalent to the PL value measured with exfoliated and synthesized single-crystal monolayer WSe_2 [5,37,39]. On the other hand, when only Ar (200 sccm) was used as a carrier gas, the PL of synthesized WSe_2 had a low intensity and showed a wide distribution due to the formation of bilayers and multilayers of WSe_2, as shown in Figure 3e. The synthesis effects of CH_4 gas were demonstrated from the representative PL spectrum of each PL mapping shown in Figure 3f. Based on these optical property data, it was confirmed that when using CH_4 as a promoter in the WSe_2 growth process, large WSe_2 grains with uniform monolayers can be synthesized.

As shown in the topology images obtained through tapping mode AFM, the thickness of the synthesized WSe_2 is uniform to ~0.7 nm, corresponding to the thickness of the monolayer (Figure 4a) [40,41]. A KPFM image of the monolayer WSe_2 showed a reduction in surface potential of ~300 meV in WSe_2 due to the electrostatic screening effect and charge distribution of WSe_2 (Figure 4b) [42]. The work function of the Pt-coated tip was ~4.3 eV, which was obtained by measuring the surface potential of highly oriented pyrolytic graphite (HOPG) (Figure S7). Since the work function of the SiO_2/Si substrate was 4.6 eV, the work function of the synthesized WSe_2 was estimated to be ~4.3 eV. This value is equivalent to the work function value of the exfoliated monolayer WSe_2 [43]. Figure 4c,d show the XPS results of the synthesized monolayer WSe_2 with four W-4f peaks ($W^{4+}4f_{7/2}$: 32.8 eV, $W^{4+}4f_{5/2}$: 34.8 eV, $W^{6+}4f_{7/2}$: 36 eV, and $W^{6+}4f_{5/2}$: 38.2 eV) and two Se-3D peaks (Se $3d_{5/2}$: 55.1 eV and $3d_{3/2}$: 55.9 eV). The two $W^{4+}4f$ peaks correspond to the binding energy of W bonded to Se atoms, while the two Se-3d peaks point to the binding energy of Se bonded to W atoms. The two $W^{6+}4f$ peaks correspond to the binding energy of the W atoms bonded to the O atoms, resulting from the exposure of the synthesized WSe_2 to air during the XPS analysis. Additionally, there was no W-4f peak at 32 eV and 34 eV, which represent the 1T phase; therefore, it can be confirmed at the WSe_2 of the 2H phase. These results are consistent with previous reports on WSe_2 [12,44].

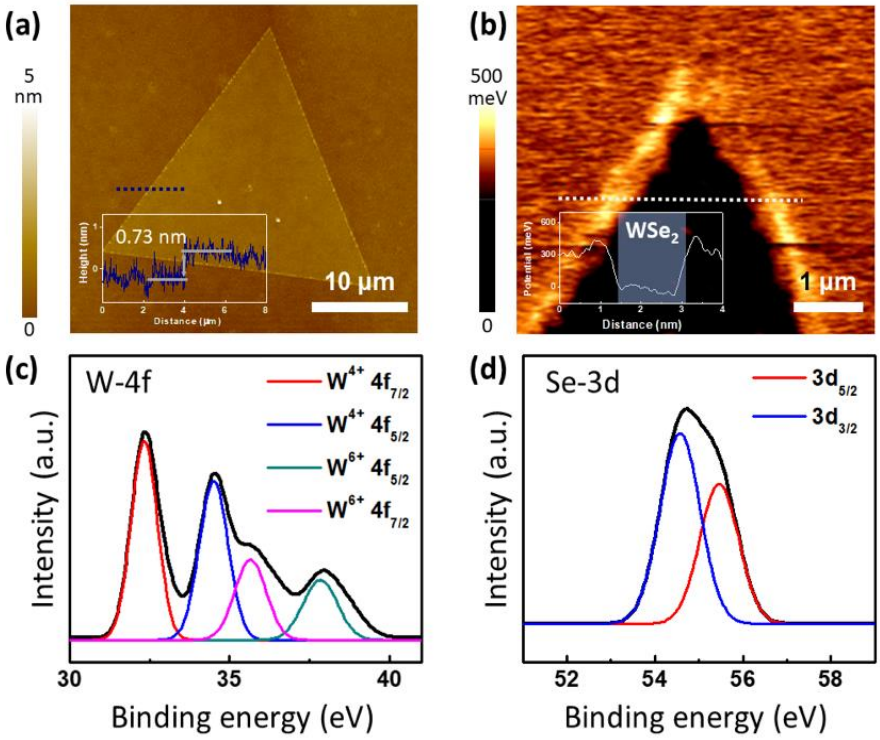

Figure 4. (**a**) Atomice force microscopy (AFM) image of the synthesized monolayer WSe_2. The inset graph is the height profile corresponding to the blue dot line. (**b**) Surface potential mapping image of WSe_2 by Kelvin probe force microscopy (KPFM). The inset graph is the surface potential profile corresponding to the white dot line. X-ray photoelectron spectroscopy (XPS) analysis of (**c**) W-4f and (**d**) Se-3d of synthesized WSe_2.

4. Conclusions

In summary, we developed a CH_4-assisted vapor transport growth method to obtain high-quality monolayer WSe_2 crystals with large domain sizes. Unlike other promoter s or growth promoters previously reported (polymer, halide, and metal), CH_4 only acts as a promoter for WSe_2 growth without producing any residue. Moreover, the nucleation density of WSe_2 was tuned (from 1.6×10^5 to 1.5×10^2 mm^{-2}) by using the gas-phase CH_4 promoter with precise flow control. The characterization of the synthesized monolayer WSe_2 by Raman, PL, and KPFM confirmed that CH_4 is a suitable candidate as a promoter for the growth of high-quality monolayer WSe_2. Finally, our CH_4-assisted growth approach may be applicable for the controlled growth of high-quality single crystals of other TMDs.

Supplementary Materials: The following are available online at http://www.mdpi.com/2079-4991/9/11/1642/s1: Figures S1–S4—The SEM results at each synthesis condition for statistical analysis, Figure S5—Distribution of grain sizes in WSe_2 according to carrier gas ratios, Figure S6—Raman spectrum of synthesized monolayer WSe_2, Figure S7—The work function of Pt-coated AFM tip and reference HOPG, and Figure S8—XPS wide-range spectra of synthesized WSe_2.

Author Contributions: H.-S.J. and J.-Y.L. contributed equally to this work. H.-S.J. and S.-G.K. synthesized the samples. J.-Y.L. and S.-K.S. analyzed and performed the scanning electron microscopy, aAFM, KPFM, and XPS. H.-S.J. and S.-H.H. measured the optical properties (Raman and PL). J.-H.L. and D.W. guided the project and analyzed the results. H.-S.J., J.-Y.L., S.S., J.-H.L., and D.W. wrote the paper. All authors participated in reviewing the manuscript. All authors approved the final version of the manuscript.

Funding: This work was supported by the Korea Basic Science Institute (KBSI) National Research Facilities and Equipment Center (NFEC) grant funded by the Korean government (Ministry of Education) (No. 2019R1A6C1010031) and the National Research Foundation of Korea (NRF) grant funded by the Korean government (MSIP) (NRF-2019R1F1A1062330) and the Ajou University research fund.

Conflicts of Interest: The authors declare no conflict of interest.

References

1. Geim, A.K. Graphene: Status and prospects. *Science* **2009**, *324*, 1530–1534. [CrossRef] [PubMed]
2. Ross, J.S.; Klement, P.; Jones, A.M.; Ghimire, N.J.; Yan, J.; Mandrus, D.G.; Taniguchi, T.; Watanabe, K.; Kitamura, K.; Yao, W.; et al. Electrically tunable excitonic light-emitting diodes based on monolayer WSe_2 p-n junctions. *Nat. Nanotechnol.* **2014**, *9*, 268–272. [CrossRef] [PubMed]
3. Baugher, B.W.; Churchill, H.O.; Yang, Y.; Jarillo-Herrero, P. Optoelectronic devices based on electrically tunable p-n diodes in a monolayer dichalcogenide. *Nat. Nanotechnol.* **2014**, *9*, 262–267. [CrossRef] [PubMed]
4. Zhang, H. Ultrathin Two-Dimensional Nanomaterials. *ACS Nano* **2015**, *9*, 9451–9469. [CrossRef]
5. Li, H.; Lu, G.; Wang, Y.; Yin, Z.; Cong, C.; He, Q.; Wang, L.; Ding, F.; Yu, T.; Zhang, H. Mechanical exfoliation and characterization of single- and few-layer nanosheets of WSe_2, TaS_2, and $TaSe_2$. *Small* **2013**, *9*, 1974–1981. [CrossRef]
6. Li, H.; Wu, J.; Yin, Z.; Zhang, H. Preparation and applications of mechanically exfoliated single-layer and multilayer MoS_2 and WSe_2 nanosheets. *Acc. Chem. Res.* **2014**, *47*, 1067–1075. [CrossRef]
7. Zhao, W.; Ghorannevis, Z.; Chu, L.; Toh, M.; Kloc, C.; Tan, P.H.; Eda, G. Evolution of electronic structure in atomically thin sheets of WS_2 and WSe_2. *ACS Nano* **2013**, *7*, 791–797. [CrossRef]
8. Terrones, H.; Lopez-Urias, F.; Terrones, M. Novel hetero-layered materials with tunable direct band gaps by sandwiching different metal disulfides and diselenides. *Sci. Rep.* **2013**, *3*, 1549. [CrossRef] [PubMed]
9. Fang, H.; Chuang, S.; Chang, T.C.; Takei, K.; Takahashi, T.; Javey, A. High-performance single layered WSe_2 p-FETs with chemically doped contacts. *Nano Lett.* **2012**, *12*, 3788–3792. [CrossRef]
10. Zhou, H.; Wang, C.; Shaw, J.C.; Cheng, R.; Chen, Y.; Huang, X.; Liu, Y.; Weiss, N.O.; Lin, Z.; Huang, Y.; et al. Large area growth and electrical properties of p-type WSe_2 atomic layers. *Nano Lett.* **2015**, *15*, 709–713. [CrossRef]
11. Gao, Y.; Hong, Y.L.; Yin, L.C.; Wu, Z.; Yang, Z.; Chen, M.L.; Liu, Z.; Ma, T.; Sun, D.M.; Ni, Z.; et al. Ultrafast Growth of High-Quality Monolayer WSe_2 on Au. *Adv. Mater.* **2017**, *29*, 1700990. [CrossRef]
12. Huang, J.; Yang, L.; Liu, D.; Chen, J.; Fu, Q.; Xiong, Y.; Lin, F.; Xiang, B.J.N. Large-area synthesis of monolayer WSe_2 on a SiO_2/Si substrate and its device applications. *Nanoscale* **2015**, *7*, 4193–4198. [CrossRef]
13. Ling, X.; Lee, Y.H.; Lin, Y.; Fang, W.; Yu, L.; Dresselhaus, M.S.; Kong, J. Role of the seeding promoter in MoS_2 growth by chemical vapor deposition. *Nano Lett.* **2014**, *14*, 464–472. [CrossRef]
14. Liu, B.; Fathi, M.; Chen, L.; Abbas, A.; Ma, Y.; Zhou, C. Chemical Vapor Deposition Growth of Monolayer WSe_2 with Tunable Device Characteristics and Growth Mechanism Study. *ACS Nano* **2015**, *9*, 6119–6127. [CrossRef]
15. Liu, J.; Zeng, M.; Wang, L.; Chen, Y.; Xing, Z.; Zhang, T.; Liu, Z.; Zuo, J.; Nan, F.; Mendes, R.G.; et al. Ultrafast Self-Limited Growth of Strictly Monolayer WSe_2 Crystals. *Small* **2016**, *12*, 5741–5749. [CrossRef]
16. Clark, G.; Wu, S.F.; Rivera, P.; Finney, J.; Nguyen, P.; Cobden, D.H.; Xu, X.D. Vapor-transport growth of high optical quality WSe_2 monolayers. *APL Mater.* **2014**, *2*, 101101. [CrossRef]
17. Elias, A.L.; Perea-Lopez, N.; Castro-Beltran, A.; Berkdemir, A.; Lv, R.; Feng, S.; Long, A.D.; Hayashi, T.; Kim, Y.A.; Endo, M.; et al. Controlled synthesis and transfer of large-area WS_2 sheets: From single layer to few layers. *ACS Nano* **2013**, *7*, 5235–5242. [CrossRef]
18. Li, M.-Y.; Shi, Y.; Cheng, C.-C.; Lu, L.-S.; Lin, Y.-C.; Tang, H.-L.; Tsai, M.-L.; Chu, C.-W.; Wei, K.-H.; He, J.-H. Epitaxial growth of a monolayer WSe_2-MoS_2 lateral pn junction with an atomically sharp interface. *Science* **2015**, *349*, 524–528. [CrossRef]
19. Park, J.; Choudhary, N.; Smith, J.; Lee, G.; Kim, M.; Choi, W. Thickness modulated MoS_2 grown by chemical vapor deposition for transparent and flexible electronic devices. *Appl. Phys. Lett.* **2015**, *106*, 012104. [CrossRef]
20. Zhan, Y.; Liu, Z.; Najmaei, S.; Ajayan, P.M.; Lou, J. Large-area vapor-phase growth and characterization of MoS_2 atomic layers on a SiO_2 substrate. *Small* **2012**, *8*, 966–971. [CrossRef]
21. Choi, W.; Choudhary, N.; Han, G.H.; Park, J.; Akinwande, D.; Lee, Y.H. Recent development of two-dimensional transition metal dichalcogenides and their applications. *Mater Today* **2017**, *20*, 116–130. [CrossRef]
22. Lee, Y.H.; Zhang, X.Q.; Zhang, W.; Chang, M.T.; Lin, C.T.; Chang, K.D.; Yu, Y.C.; Wang, J.T.; Chang, C.S.; Li, L.J.; et al. Synthesis of large-area MoS_2 atomic layers with chemical vapor deposition. *Adv. Mater.* **2012**, *24*, 2320–2325. [CrossRef]

23. Liu, K.K.; Zhang, W.; Lee, Y.H.; Lin, Y.C.; Chang, M.T.; Su, C.Y.; Chang, C.S.; Li, H.; Shi, Y.; Zhang, H.; et al. Growth of large-area and highly crystalline MoS_2 thin layers on insulating substrates. *Nano Lett.* **2012**, *12*, 1538–1544. [CrossRef]
24. Shi, Y.; Zhou, W.; Lu, A.Y.; Fang, W.; Lee, Y.H.; Hsu, A.L.; Kim, S.M.; Kim, K.K.; Yang, H.Y.; Li, L.J.; et al. van der Waals epitaxy of MoS_2 layers using graphene as growth templates. *Nano Lett.* **2012**, *12*, 2784–2791. [CrossRef]
25. Lee, Y.H.; Yu, L.; Wang, H.; Fang, W.; Ling, X.; Shi, Y.; Lin, C.T.; Huang, J.K.; Chang, M.T.; Chang, C.S.; et al. Synthesis and transfer of single-layer transition metal disulfides on diverse surfaces. *Nano Lett.* **2013**, *13*, 1852–1857. [CrossRef]
26. Wu, S.; Huang, C.; Aivazian, G.; Ross, J.S.; Cobden, D.H.; Xu, X. Vapor-solid growth of high optical quality MoS_2 monolayers with near-unity valley polarization. *ACS Nano* **2013**, *7*, 2768–2772. [CrossRef]
27. Li, S.S.; Wang, S.F.; Tang, D.M.; Zhao, W.J.; Xu, H.L.; Chu, L.Q.; Bando, Y.; Golberg, D.; Eda, G. Halide-assisted atmospheric pressure growth of large WSe_2 and WS_2 monolayer crystals. *App.l Mater. Today* **2015**, *1*, 60–66. [CrossRef]
28. Cantelo, R.C. The Thermal Decomposition of Methane. *J. Phys. Chem. A* **1924**, *28*, 1036–1048. [CrossRef]
29. Permenov, D.G.; Radzig, V.A. Mechanisms of Heterogeneous Processes in the System SiO_2 + CH_4: II. Methylation of >Si=O Groups. *Kinet. Catal.* **2004**, *45*, 265–272. [CrossRef]
30. Zhang, F.; Su, D.; He, J.; Sang, Z.; Liu, Y.; Ma, Y.; Liu, R.; Yan, X. Methyl modified SiO_2 aerogel with tailored dual modal pore structure for adsorption of organic solvents. *Mater. Lett.* **2019**, *238*, 202–205. [CrossRef]
31. Li, X.; Li, X.; Zang, X.; Zhu, M.; He, Y.; Wang, K.; Xie, D.; Zhu, H. Role of hydrogen in the chemical vapor deposition growth of MoS_2 atomic layers. *Nanoscale* **2015**, *7*, 8398–8404. [CrossRef] [PubMed]
32. Lee, J.H.; Lee, E.K.; Joo, W.J.; Jang, Y.; Kim, B.S.; Lim, J.Y.; Choi, S.H.; Ahn, S.J.; Ahn, J.R.; Park, M.H.; et al. Wafer-scale growth of single-crystal monolayer graphene on reusable hydrogen-terminated germanium. *Science* **2014**, *344*, 286–289. [CrossRef] [PubMed]
33. Geng, D.; Wu, B.; Guo, Y.; Huang, L.; Xue, Y.; Chen, J.; Yu, G.; Jiang, L.; Hu, W.; Liu, Y. Uniform hexagonal graphene flakes and films grown on liquid copper surface. *Proc. Nat. Acad. Sci. USA* **2012**, *109*, 7992–7996. [CrossRef] [PubMed]
34. Wang, L.; Xu, X.; Zhang, L.; Qiao, R.; Wu, M.; Wang, Z.; Zhang, S.; Liang, J.; Zhang, Z.; Zhang, Z.; et al. Epitaxial growth of a 100-square-centimetre single-crystal hexagonal boron nitride monolayer on copper. *Nature* **2019**, *570*, 91–95. [CrossRef]
35. Chen, S.; Ji, H.; Chou, H.; Li, Q.; Li, H.; Suk, J.W.; Piner, R.; Liao, L.; Cai, W.; Ruoff, R.S. Millimeter-size single-crystal graphene by suppressing evaporative loss of Cu during low pressure chemical vapor deposition. *Adv. Mater.* **2013**, *25*, 2062–2065. [CrossRef]
36. Lee, J.S.; Choi, S.H.; Yun, S.J.; Kim, Y.I.; Boandoh, S.; Park, J.-H.; Shin, B.G.; Ko, H.; Lee, S.H.; Kim, Y.-M.; et al. Wafer-scale single-crystal hexagonal boron nitride film via self-collimated grain formation. *Science* **2018**, *362*, 817–821. [CrossRef]
37. Tonndorf, P.; Schmidt, R.; Bottger, P.; Zhang, X.; Borner, J.; Liebig, A.; Albrecht, M.; Kloc, C.; Gordan, O.; Zahn, D.R.; et al. Photoluminescence emission and Raman response of monolayer MoS_2, $MoSe_2$, and WSe_2. *Opt. Mater. Express* **2013**, *21*, 4908–4916. [CrossRef]
38. Pham, V.P.; Jang, H.S.; Whang, D.; Choi, J.Y. Direct growth of graphene on rigid and flexible substrates: Progress, applications, and challenges. *Chem. Soc. Rev.* **2017**, *46*, 6276–6300. [CrossRef]
39. Zeng, H.; Liu, G.B.; Dai, J.; Yan, Y.; Zhu, B.; He, R.; Xie, L.; Xu, S.; Chen, X.; Yao, W.; et al. Optical signature of symmetry variations and spin-valley coupling in atomically thin tungsten dichalcogenides. *Sci. Rep.* **2013**, *3*, 1608. [CrossRef]
40. Wang, K.; Huang, B.; Tian, M.; Ceballos, F.; Lin, M.W.; Mahjouri-Samani, M.; Boulesbaa, A.; Puretzky, A.A.; Rouleau, C.M.; Yoon, M.; et al. Interlayer Coupling in Twisted WSe_2/WS_2 Bilayer Heterostructures Revealed by Optical Spectroscopy. *ACS Nano* **2016**, *10*, 6612–6622. [CrossRef]
41. Almadori, Y.; Bendiab, N.; Grevin, B. Multimodal Kelvin Probe Force Microscopy Investigations of a Photovoltaic WSe_2/MoS_2 Type-II Interface. *ACS Appl. Mater. Interfaces* **2018**, *10*, 1363–1373. [CrossRef] [PubMed]
42. Li, F.; Qi, J.; Xu, M.; Xiao, J.; Xu, Y.; Zhang, X.; Liu, S.; Zhang, Y. Layer Dependence and Light Tuning Surface Potential of 2D MoS_2 on Various Substrates. *Small* **2017**, *13*, 1603103. [CrossRef] [PubMed]

43. Britnell, L.; Ribeiro, R.M.; Eckmann, A.; Jalil, R.; Belle, B.D.; Mishchenko, A.; Kim, Y.J.; Gorbachev, R.V.; Georgiou, T.; Morozov, S.V.; et al. Strong light-matter interactions in heterostructures of atomically thin films. *Science* **2013**, *340*, 1311–1314. [CrossRef] [PubMed]
44. Tao, L.; Meng, F.; Zhao, S.; Song, Y.; Yu, J.; Wang, X.; Liu, Z.; Wang, Y.; Li, B.; Wang, Y.J.N. Experimental and theoretical evidence for the ferromagnetic edge in WSe_2 nanosheets. *Nanoscale* **2017**, *9*, 4898–4906. [CrossRef] [PubMed]